Weather Clim. Dynam., 7, 2251–2266, 2026
https://doi.org/10.5194/wcd-7-2251-2026
© Author(s) 2026. This work is distributed under
the Creative Commons Attribution 4.0 License.

Weather and Climate Dynamics
Open Access
EGU

Two distinct modes of North American spring temperature evolution shaped by tropical SST regimes and midlatitude circulation

Wogu Zhong[1,2], **Mingfang Ting**[2], **and Zhiwei Wu**[1,3]

[1]Department of Atmospheric and Oceanic Sciences & Institute of Atmospheric Sciences/Key Laboratory of Polar Atmosphere-ocean-ice System for Weather and Climate, Ministry of Education/Shanghai Key Laboratory of Ocean-land-atmosphere Boundary Dynamics and Climate Change, Fudan University, Shanghai, 200438, China
[2]Lamont-Doherty Earth Observatory, Columbia University, Palisades, New York, 10964, United States of America
[3]IRDR ICoE on Risk Interconnectivity and Governance on Weather/Climate Extremes Impact and Public Health, Fudan University, Shanghai, 200438, China

Correspondence: Wogu Zhong (wz2758@columbia.edu, wgzhong19@fudan.edu.cn) and Mingfang Ting (ting@ldeo.columbia.edu)

Received: 23 May 2026 – Discussion started: 11 June 2026
Revised: 29 September 2026 – Accepted: 30 October 2026 – Published: 12 November 2026

Abstract. Abnormal temperature fluctuations during spring can substantially impact vegetation growth, agricultural productivity, and ecosystem stability. However, the physical processes underlying year-to-year variations in the evolution of North American spring temperature anomalies remain poorly understood. Here, we apply Season-reliant Empirical Orthogonal Function (S-EOF) analysis to identify the leading modes of spring temperature evolution over North America. We focus on the first two modes here, which differ from conventional responses to winter El Niño–Southern Oscillation (ENSO) and are instead linked to distinct evolutions of tropical sea surface temperature (SST). The first mode (S-EOF1) features rapidly decaying Eastern Pacific (EP) ENSO-like SST anomalies from winter to spring and the emergence of tropical North Atlantic (TNA) SST anomalies, accompanied by a persistent north–south temperature dipole over North America. This mode is jointly influenced by the North Pacific Oscillation (NPO) and TNA-related North Atlantic circulation anomalies. In contrast, the second mode (S-EOF2) is associated with more persistent Central Pacific (CP) ENSO-like SST anomalies and the absence of TNA SST anomalies, together with evolving temperature patterns with temporal phase reversals across large parts of North America. This mode is primarily associated with the North Pacific (NP) pattern, whose influence may be further amplified by persistent CP ENSO-like SST anomalies. Dominance analysis further quantifies the relative contributions of tropical SST and midlatitude circulation patterns. These findings highlight the critical roles of ENSO decay rate and spatial structure, TNA SST variability, and their coupling with midlatitude circulation in shaping distinct spring temperature evolution patterns, with important implications for improving seasonal prediction.

1 Introduction

As a transition season between boreal winter and summer, spring over North America is marked by pronounced interannual and subseasonal temperature variability (Schwartz and Reiter, 2000). With the seasonal northward shift of solar radiation, surface energy input increases rapidly, facilitated by declining snow cover and associated albedo feedbacks (Diro et al., 2018). At the same time, cold air masses over the Arctic remain active and can still penetrate into the midlatitudes under favorable circulation patterns. The interplay between increasing radiative forcing and intermittent cold air outbreaks often promotes "false spring" conditions, leading to rapid swings between warm and cold temperatures (Chamberlain et al., 2019). Such temperature variability can directly influence vegetation growth, thereby modulating terrestrial carbon uptake (Byrne et al., 2020; Mekonnen et al., 2016; Wang et al., 2011). In addition, late-spring frost events can significantly reduce yields and disrupt productivity (Leduc and Logan, 2025). Spring temperature fluctuations can also

influence hydrological processes, shift species distributions, and increase the likelihood of extreme events (Barcikowska et al., 2019; Choi and Kim, 2018; McDonald et al., 2012; Seager and Vecchi, 2010; Xue et al., 2018). Therefore, understanding the characteristics and underlying mechanisms of North American spring temperature variability is essential for improving both climate prediction and decision-making in agriculture and ecosystem management.

North American spring temperature variability is inherently linked to midlatitude circulation patterns over both the upstream (North Pacific) and downstream (North Atlantic) regions. For example, the North Pacific Oscillation (NPO), a basin-wide meridional seesaw pattern over the North Pacific, can modulate the anticyclonic ridge near Alaska and thereby influence cold air outbreaks over North America (Ji et al., 2024; Sung et al., 2019). The North Atlantic Oscillation (NAO), on the other hand, influences North American temperature variability by altering the strength and preferred location of the westerly jet stream and storm tracks over the North Atlantic (Abatzoglou and Redmond, 2007; Ault et al., 2011; Hurrell, 1995; Soulard and Lin, 2017). These circulation patterns can also be regulated or reinforced by tropical sea surface temperature (SST) anomalies. The El Niño–Southern Oscillation (ENSO) can excite the Pacific–North American (PNA) pattern and modulate the strength of the Aleutian Low (commonly measured by the North Pacific, NP, index (Trenberth and Hurrell, 1994)), thereby influencing North American spring climate (Chen et al., 2020; Ding et al., 2025; Jong et al., 2020; Sun et al., 2019; Wang et al., 2020). In addition, air–sea interactions over the North Pacific may further enhance an NPO-like pattern and exert significant impacts on North American temperature variability (Ji and Ding, 2023; Park et al., 2017). SST anomalies in the tropical western Pacific can also influence North American spring climate by generating large-scale teleconnections that propagate across the North Pacific (He and Yang, 2018; Wei et al., 2023). Apart from Pacific SST variability, tropical Atlantic SST anomalies have been shown to play an important role in shaping North American spring temperature anomalies by inducing an NAO-like response in the North Atlantic (Fu et al., 2025; Hou et al., 2023; Sheng et al., 2023). The coupling between the NPO and NAO may further amplify their impacts on North American spring temperatures (Ji et al., 2025).

Despite the transitional nature of the spring season, previous studies have primarily focused on seasonal mean temperature variability. However, the timing of spring onset has been shown to be more sensitive to large-scale circulation patterns on monthly scales (Ault et al., 2011). A weakening of the spring Aleutian Low in recent decades (Sun et al., 2019), combined with enhanced atmospheric waviness (Fragkoulidis et al., 2018), may lead to larger and more frequent subseasonal temperature swings. These features highlight the importance of understanding spring temperature variability beyond the seasonal mean, particularly at subseasonal time scales (Breeden et al., 2022; Hwang et al., 2025). Recent studies have applied the Season-reliant Empirical Orthogonal Function (S-EOF) analysis (Wang and An, 2005) to identify the dominant month-to-month evolution patterns of Eurasian winter temperature variability (Zhong and Wu, 2022, 2023, 2024). In this study, we extend the S-EOF analysis to revisit North American spring temperature variability, with a particular focus on its month-to-month evolution, and to elucidate the roles of tropical SST and midlatitude circulation patterns.

The rest of this paper is structured as follows. Section 2 introduces the data and methods used in this study. Section 2.1 describes the reanalysis datasets and climate indices, while Sect. 2.2 and 2.3 present the S-EOF analysis used to identify North American spring temperature evolution patterns and the dominance analysis employed to quantify the relative importance of different climate indices, respectively. Section 3 presents the main results. Section 3.1 describes two distinct spring temperature evolution patterns over North America and their associated circulation anomalies. Section 3.2 explores their connections with tropical SST regimes and midlatitude circulation through the Atlantic and Pacific pathways. Section 3.3 quantifies the relative contributions of tropical SST variability and midlatitude circulation using dominance analysis. Finally, Sect. 4 summarizes the main conclusions and discusses several implications of the findings.

2 Data and methods

2.1 Data and indices

This study utilizes monthly ERA5 reanalysis data (Hersbach et al., 2020) provided by the European Centre for Medium-Range Weather Forecasts (ECMWF). All surface and pressure-level variables are regridded from the original horizontal resolution of $0.25° \times 0.25°$ to $2.5° \times 2.5°$. In addition, monthly SST data from the National Oceanic and Atmospheric Administration (NOAA) Extended Reconstructed SST version 5 (ERSST v5, Huang et al., 2017) are used, with a horizontal resolution of $2° \times 2°$.

The Niño3.4 index is defined as the area-averaged SST anomalies over the Niño3.4 region (5° N–5° S, 170–120° W). The Eastern Pacific (EP) ENSO index (EPI) and Central Pacific (CP) ENSO index (CPI) are derived from the first two EOF modes of winter-mean SST anomalies over the equatorial Pacific (15° S–15° N, 140° E–80° W). The EPI is defined as $(\text{SST-PC1} - \text{SST-PC2})/\sqrt{2}$, whereas the CPI is defined as $(\text{SST-PC1} + \text{SST-PC2})/\sqrt{2}$, where SST-PC1 and SST-PC2 denote the standardized principal components (PCs) of the first two SST EOF modes (Geng et al., 2022; Takahashi et al., 2011). The Indian Ocean Dipole (IOD) index is defined as the difference in SST anomalies between the western equatorial Indian Ocean (10° S–10° N, 50–70° E) and the southeastern equatorial Indian Ocean (10° S–0°, 90–110° E)

(Saji et al., 1999). The NP index is defined as the negative of the area-weighted sea level pressure (SLP) over the North Pacific (30–65° N, 160° E–140° W); thus, a positive NP index corresponds to a deepened Aleutian Low during the cold season, and vice versa (Trenberth and Hurrell, 1994). The NPO index is calculated as the difference in SLP anomalies between the southern (10°–30° N, 180°–135° W) and northern (50°–75° N, 175°–115° W) regions of the North Pacific (Hu et al., 2024). The station-based NAO index is defined as the normalized pressure difference between Gibraltar and southwestern Iceland, as maintained by the Climatic Research Unit at the University of East Anglia (Jones et al., 1997). This study focuses on the spring season spanning 1941–2024. Since winter ENSO includes December of the preceding year, data from December 1940 are also included. All data and fields are linearly detrended prior to analysis.

2.2 S-EOF analysis

The S-EOF analysis is an objective method used to separate modes of climate variability that depend on the seasonal cycle (Wang and An, 2005; Zhong and Wu, 2022). In this study, the S-EOF analysis is performed by constructing an extended data matrix in which monthly surface air temperature (SAT) anomalies over North America within the spring season (March–April–May) are concatenated into a single state vector:

$$X_{3m\times n} = \begin{matrix} X_{1,1}^{\mathrm{Mar}} & \cdots & X_{1,n}^{\mathrm{Mar}} \\ \vdots & \ddots & \vdots \\ X_{m,1}^{\mathrm{Mar}} & \cdots & X_{m,n}^{\mathrm{Mar}} \\ X_{1,1}^{\mathrm{Apr}} & \cdots & X_{1,n}^{\mathrm{Apr}} \\ \vdots & \ddots & \vdots \\ X_{m,1}^{\mathrm{Apr}} & \cdots & X_{m,n}^{\mathrm{Apr}} \\ X_{1,1}^{\mathrm{May}} & \cdots & X_{1,n}^{\mathrm{May}} \\ \vdots & \ddots & \vdots \\ X_{m,1}^{\mathrm{May}} & \cdots & X_{m,n}^{\mathrm{May}} \end{matrix} \quad (1)$$

where m denotes the number of grid points and n denotes the number of years.

To account for latitudinal area distortion, SAT anomalies are weighted by the square root of the cosine of latitude. The monthly data are then linearly detrended at each grid point to remove long-term trends. In addition, to focus on temperature variability over land, SAT anomalies over the ocean are masked out. The S-EOF analysis is then conducted based on the following correlation matrix:

$$R = \frac{1}{n-1}\tilde{\mathbf{X}}\tilde{\mathbf{X}}^T \quad (2)$$

where $\tilde{\mathbf{X}}$ denotes the standardized data matrix.

The eigenvalue problem is solved as:

$$R\mathbf{e}_k = \lambda_k \mathbf{e}_k \quad (3)$$

where λ_k is the eigenvalue corresponding to the k-th S-EOF mode, indicating the fraction of explained variance, and $\mathbf{e}_k = \left[\mathbf{e}_{1,k}^{\mathrm{Mar}}, \cdots, \mathbf{e}_{m,k}^{\mathrm{Mar}}, \mathbf{e}_{1,k}^{\mathrm{Apr}}, \cdots, \mathbf{e}_{m,k}^{\mathrm{Apr}}, \mathbf{e}_{1,k}^{\mathrm{May}}, \cdots, \mathbf{e}_{m,k}^{\mathrm{May}}\right]$ represents the associated S-EOF spatial pattern with explicit monthly evolution.

The corresponding PCs are obtained by projecting the standardized data onto the eigenvectors, yielding one value per year:

$$\mathrm{PC}_k = \tilde{X}^T \mathbf{e}_k \quad (4)$$

2.3 Dominance analysis

Dominance analysis is a Shapley value-based framework used to assess the relative importance of variables in multiple regression models (Azen and Budescu, 2003; Grömping, 2007; Shapley, 1953). It quantifies the weighted-average incremental contribution to the explained variance (R^2) across all possible subset models that exclude X_j. The contribution of X_j is given by:

$$C_j = \sum_{A\subseteq S\setminus\{X_j\}} \frac{|A|!\,(p-|A|-1)!}{p!} \left[R^2\left(A\cup\{X_j\}\right) - R^2(A)\right] \quad (5)$$

where S denotes the full set of variables, A represents any subset of variables excluding X_j, and p is the total number of variables.

Dominance analysis ensures that the sum of the contributions of all individual variables equals the R^2 of the complete model (i.e., the model including all variables). In other words, the total R^2 can be uniquely decomposed and attributed to each variable, effectively mitigating the impacts of multicollinearity among variables (Azen and Budescu, 2003; Grömping, 2007).

Based on the physical interpretation of the S-EOF modes in the following analysis, six indices are selected to construct regression models for each PC. To quantify their relative importance, a total of $2^6 = 64$ regression models (including the null model) are considered. For example, to evaluate the contribution of the winter EPI to S-EOF1, all subset models excluding this index (regression models 1–32, a total of $2^5 = 32$ regression models, representing all combinations of the remaining five indices) are first constructed. The weighted-average R^2 of these models in explaining PC1 is taken as the baseline. Then, the winter EPI is added to each of these subset models, generating another set of 32 regression models (regression models 33–64). The weighted-average increase in R^2 across all model pairs, represents the contribution of the winter EPI to S-EOF1. The same procedure is applied to all other indices to quantify their relative contributions.

The uncertainty of the dominance analysis is assessed using a bootstrap procedure. Specifically, years are randomly resampled with replacement while maintaining the same

sample size as the original analysis period (84 years). The dominance analysis is repeated for each of the 10 000 bootstrap samples, and the 5th and 95th percentiles of the resulting distributions are used to quantify the uncertainty.

3 Results

3.1 Distinct spring temperature evolution patterns

Figure 1 presents the climatological spring SAT, SLP, and 925 hPa winds. Over North America, SAT generally decreases with latitude, while the meridional temperature gradient weakens from March (Fig. 1a) to May (Fig. 1c). In the SLP field, both the North Pacific and North Atlantic sectors exhibit a meridional dipole characterized by a subpolar low and a subtropical high. From March (Fig. 1a) to May (Fig. 1c), the subpolar lows weaken while the subtropical highs strengthen in response to the seasonal northward shift of solar radiation. The combined influence of the Aleutian Low and Icelandic Low favors an atmospheric ridge and northwesterly winds over northern North America, particularly in March (Fig. 1a), although the ridge and associated winds weaken by May (Fig. 1c). In contrast, the North Pacific subtropical high and the Azores High favor an atmospheric trough and southerly winds over southern North America, both of which gradually intensify from March (Fig. 1a) to May (Fig. 1c). In addition, the meridional dipole structures over the North Pacific and North Atlantic sectors induce midlatitude westerlies extending from the Gulf of Alaska into central North America and from eastern North America toward the subpolar North Atlantic. These westerlies gradually weaken from March (Fig. 1a) to May (Fig. 1c). Overall, North American SAT is jointly influenced by circulation patterns over both the North Pacific and North Atlantic sectors and is strongly modulated by the seasonal cycle.

The first two S-EOF modes of North American spring SAT anomalies are shown in Fig. 2. These two modes are well separated according to the rule of North (North et al., 1982). S-EOF1 features a north–south temperature dipole pattern, with the positive phase associated with warm anomalies in the northern part and cold anomalies to the south (Fig. 2a–c). This dipole pattern persists throughout the spring season. S-EOF2 exhibits evolving temperature patterns across the spring months, with the positive phase characterized by a westward retreat of warm anomalies and the development of widespread cold anomalies across North America from March to May (Fig. 2d–f).

The PCs of these two S-EOF modes exhibit pronounced interannual variability (Fig. 2g) and are both positively correlated with the winter Niño3.4 index, with correlation coefficients of 0.32 and 0.37, respectively. The linkages between these S-EOF modes and winter ENSO are further examined in the following section.

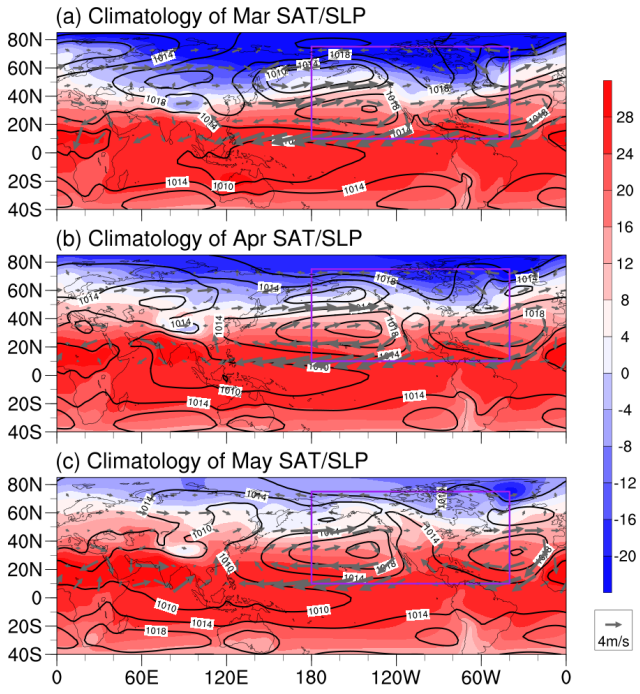


Figure 1. Climatology of SAT (shading; unit: °C), SLP (black contours; unit: hPa; at intervals of 4 hPa), and 925 hPa winds (vectors; unit: $m\,s^{-1}$; vectors plotted only between 10 and 75° N) in **(a)** March, **(b)** April, and **(c)** May. The purple box outlines North America.

S-EOF1 is associated with significant and persistent circulation anomalies over both the North Pacific and North Atlantic sectors (Fig. 3b–d). In March, a negative SLP anomaly extends from the Bering Strait to Alaska, accompanied by a negative phase of an NAO-like pattern over the North Atlantic (Fig. 3b). This circulation pattern favors wind anomalies from both the Pacific and Atlantic Oceans toward the North American continent. Over central North America, southerly wind anomalies associated with the eastern flank of the anomalous low weaken the climatological northerlies (Fig. 1a), favoring local warmer conditions. In addition, the southern center of the NAO-like pattern generates northeasterly wind anomalies over the southwestern United States, which oppose the climatological southwesterlies (Fig. 1a) and contribute to regional cooling. The loading centers of circulation anomalies remain largely stationary from March to May (Fig. 3b–d), with a slight weakening trend, and thus provide favorable conditions for a phase-locked north–south temperature dipole over North America.

In contrast, S-EOF2 is primarily associated with circulation anomalies over the North Pacific, while anomalies over the North Atlantic are only evident in March and extend farther east toward Eurasia (Fig. 3f). The anomalous low over the Bering Sea–Gulf of Alaska propagates southeastward from March to May, accompanied by the development of an anomalous high over the North American Arctic,

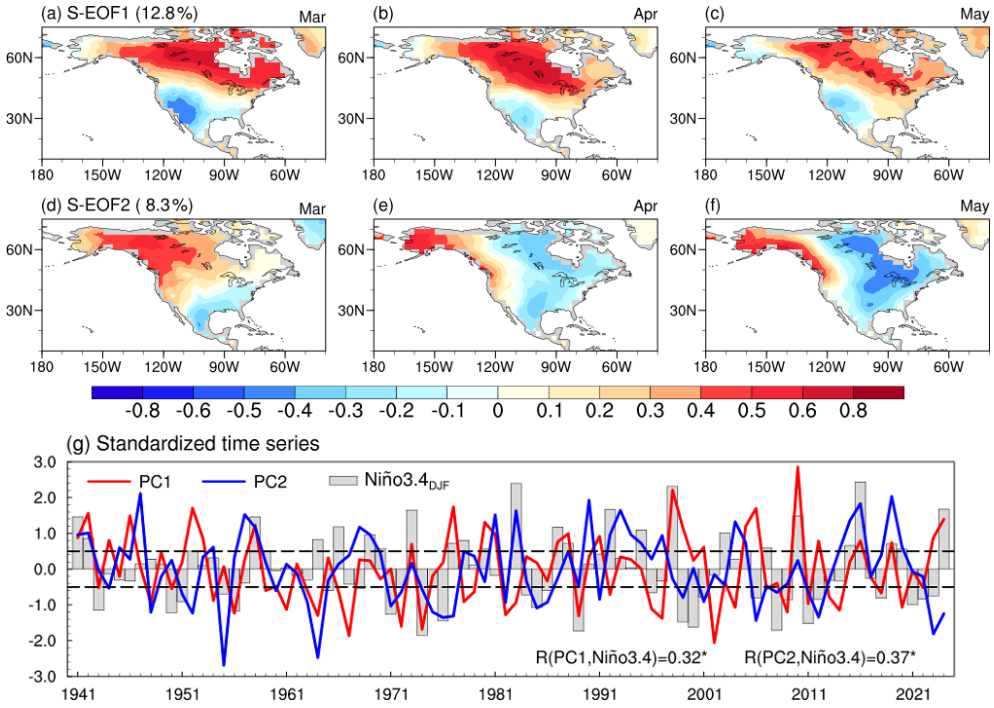


Figure 2. (a–c) The first S-EOF mode (S-EOF1) of North American spring SAT anomalies during 1941–2024, derived from a correlation matrix (shading; unitless). SAT anomalies are linearly detrended at each grid point prior to the S-EOF analysis. Panels **(a–c)** show the correlation coefficients between S-EOF1 and the detrended SAT anomalies in **(a)** March, **(b)** April, and **(c)** May, respectively. **(d–f)** Same as **(a–c)**, but for the second S-EOF mode (S-EOF2). **(g)** Standardized time series of the winter (December–January–February) Niño3.4 index (bars) and the PCs of S-EOF1 (PC1; red line) and S-EOF2 (PC2; blue line). Horizontal dashed lines denote ±0.5 standard deviations. Numbers at the bottom of panel **(g)** indicate the correlation coefficients between the PCs and the winter Niño3.4 index.

particularly in April and May (Fig. 3f–h). This anomalous high strengthens northerly wind anomalies over central North America, reinforcing the climatological northerlies (Fig. 1b, c), and thereby leads to widespread cold anomalies over central North America and temporal phase reversals of spring temperature anomalies.

Overall, the persistent temperature evolution associated with S-EOF1 is jointly regulated by circulation anomalies over both the North Pacific and North Atlantic sectors, whereas the evolving temperature pattern associated with S-EOF2 is primarily influenced by variability over the North Pacific sector.

3.2 Linkages with tropical SST regimes and midlatitude circulation

To further examine the underlying physical mechanism of these two S-EOF modes, we first investigate their potential linkages with ENSO, which has been widely documented to play a vital role in shaping North American temperature variability during the cold season (Chen et al., 2020; Ji et al., 2024; Jong et al., 2020; Zhang and Jiang, 2023). While both modes exhibit a common positive correlation with winter Niño3.4 index (Table 1), they are associated with distinct tropical SST evolutions and different spatial structures, as illustrated by Hovmöller diagrams of tropical SST anomalies regressed onto the two PCs (Fig. 4a, b). S-EOF1 is accompanied by a fast-decaying ENSO-like SST pattern from winter to spring (Fig. 4a), with the correlation between PC1 and the Niño3.4 index decreasing from 0.32 in winter to 0.25 in spring (Table 1). In contrast, S-EOF2 is associated with a slow-decaying ENSO-like SST pattern, with SST anomalies persisting into the summer (Fig. 4b). Consistently, the correlation between PC2 and the Niño3.4 index increases from 0.37 in winter to 0.44 in spring (Table 1). In addition, PC1 is significantly correlated with the EPI (i.e., EP ENSO index; $r = 0.34$), but not with the CPI (i.e., CP ENSO index), whereas PC2 is significantly correlated with the CPI ($r = 0.45$), but not with the EPI (Table 1; Fig. S3). The contrasting ENSO decay rates associated with the two modes (Fig. 4a, b) are also broadly consistent with the evolution patterns of EP and CP ENSO (Fig. S4). Such contrasting persistence characteristics have also been documented in previous studies, with EP ENSO tending to exhibit a more pronounced spring persistence barrier, whereas CP ENSO generally retains greater persistence into late spring (Kao and Yu, 2009; Lee et al., 2014; Ren et al., 2016). However, the relationships between EP/CP ENSO and the two S-EOF modes should be

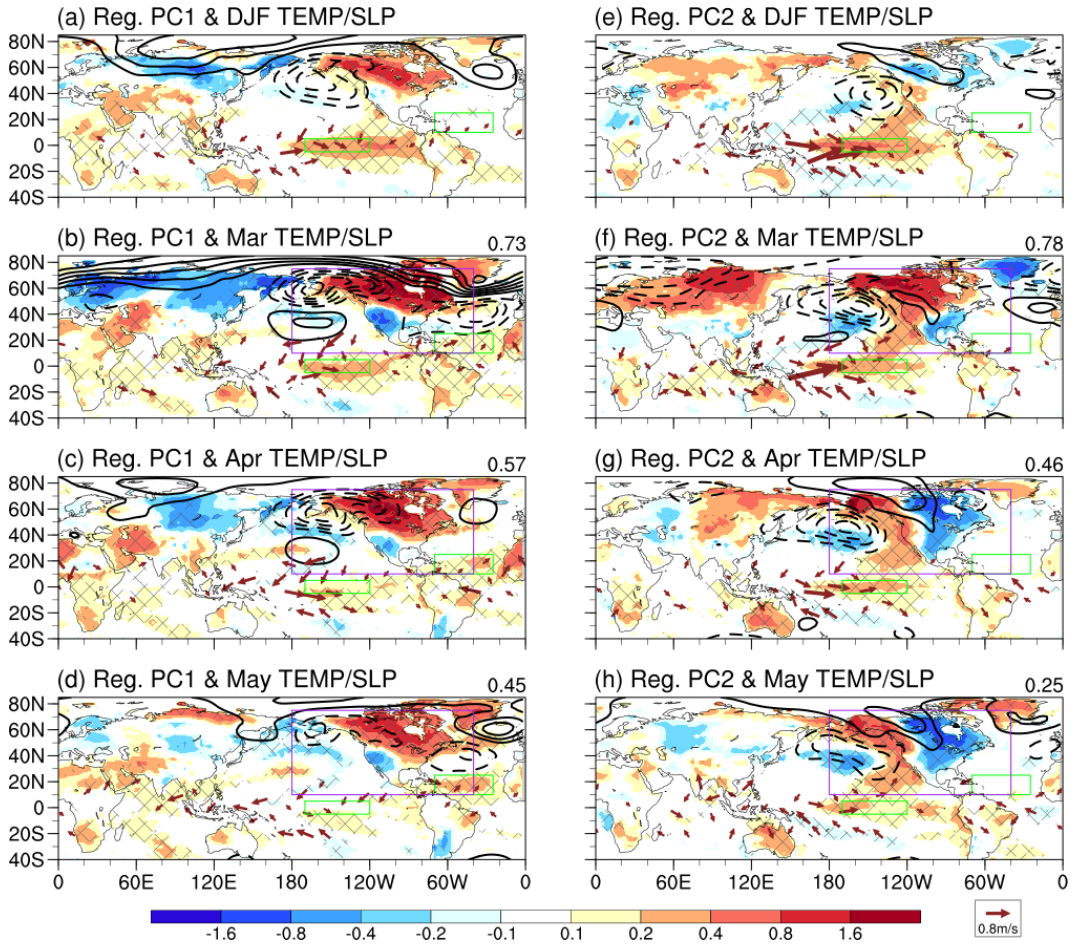


Figure 3. **(a)** Winter-mean temperature anomalies (shading; unit: °C per standard deviation of PC; with SST over ocean and SAT over land), SLP anomalies (black contours; unit: hPa per standard deviation of PC; 0.5 hPa interval with zero contour omitted), and 925 hPa wind anomalies (vectors; unit: $\mathrm{m\,s^{-1}}$ per standard deviation of PC; vectors plotted only in the tropics) regressed onto the standardized PC1. All fields are linearly detrended prior to regression. Cross-hatching indicates regions where the regressed temperature anomalies are significant at the 95 % confidence level based on a two-tailed Student's t test. Green boxes over the Pacific and Atlantic Oceans denote the Niño3.4 and TNA regions, respectively. **(b–d)** Same as **(a)**, but for anomalies in **(b)** March, **(c)** April, and **(d)** May. The purple box outlines North America. Numbers in the top-right corner of each panel indicate the pattern correlation coefficients between North American SAT anomalies regressed onto the standardized PC1 and those regressed onto the standardized winter Niño3.4 index. **(e–h)** Same as **(a–d)**, but for anomalies regressed onto the standardized PC2.

interpreted with caution, particularly for EP ENSO, as will be discussed further in the following sections.

Another key difference lies in the behavior of spring TNA SST. For S-EOF1, pronounced and statistically significant positive SST anomalies emerge over the tropical Atlantic following the El Niño-like conditions in the tropical Pacific (Fig. 4a), especially over the TNA region (Fig. 3b–d, green box over the Atlantic). Notably, no significant SST anomalies are observed over the TNA region for S-EOF2 (Fig. 3f–h), in line with the absence of pronounced circulation anomalies over the North Atlantic sector.

The differences over the Indian Ocean are less apparent in the tropical SST evolutions associated with the two S-EOF modes (Fig. 4a, b). Nevertheless, the spring IOD (i.e., Indian Ocean Dipole) index is significantly correlated with PC1 but not with PC2 (Table 1). The spring IOD index is not significantly correlated with either the winter or spring Niño3.4 index or with spring TNA SST (Table 1), suggesting that Indian Ocean variability may provide an additional contribution to the S-EOF1-related temperature evolution that is at least partly independent of tropical Pacific and Atlantic SST variability.

It is also worth noting that tropical SST evolutions associated with these two modes differ from that linked to the winter Niño3.4 index (Fig. 4c). The conventional ENSO-related spring temperature evolution does not resemble either S-EOF mode (Fig. 5a–c), but is instead more similar to a linear combination of them (Fig. 5d–f). These results suggest that trop-

Table 1. Correlation coefficients among PC1, PC2, the winter and spring Niño3.4 indices, the winter EPI and CPI, and the spring TNA, IOD, NPO, and NP indices, together with the early spring (March) NAO index. All indices are standardized and linearly detrended. Correlations significant at the 95 % confidence level based on a two-tailed Student's *t* test are shown in bold.

	PC1	PC2	Niño3.4 (DJF)	Niño3.4 (MAM)	EPI (DJF)	CPI (DJF)	TNA (MAM)	IOD (MAM)	NPO (MAM)	NP (MAM)	NAO (Mar)
PC1	**1.00**										
PC2	0.00	**1.00**									
Niño3.4 (DJF)	**0.32**	**0.37**	**1.00**								
Niño3.4 (MAM)	**0.25**	**0.44**	**0.81**	**1.00**							
EPI (DJF)	**0.34**	0.06	**0.67**	**0.53**	**1.00**						
CPI (DJF)	0.16	**0.45**	**0.71**	**0.61**	0.00	**1.00**					
TNA (MAM)	**0.40**	0.18	**0.55**	**0.45**	**0.29**	**0.46**	**1.00**				
IOD (MAM)	**0.26**	−0.16	−0.10	−0.01	−0.07	−0.04	0.06	**1.00**			
NPO (MAM)	**0.62**	−0.16	0.13	−0.05	**0.35**	−0.13	0.09	**0.31**	**1.00**		
NP (MAM)	**0.23**	**0.59**	0.18	**0.29**	0.08	**0.22**	0.09	−0.03	**0.24**	**1.00**	
NAO (Mar)	**−0.24**	**0.23**	0.11	0.18	0.10	0.03	**−0.25**	−0.11	−0.14	−0.03	**1.00**

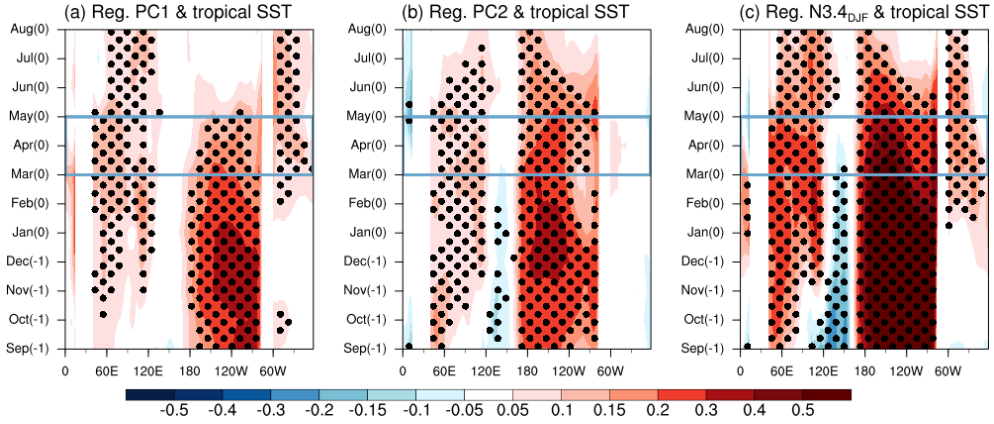


Figure 4. Hovmöller diagrams of tropical SST anomalies (shading; unit: °C per standard deviation of PC, averaged over 10° S–10° N) regressed onto **(a)** the standardized PC1, **(b)** the standardized PC2, and **(c)** the standardized winter Niño3.4 index. Dots indicate regions where the regressed SST anomalies are significant at the 95 % confidence level based on a two-tailed Student's *t* test.

ical SST regimes, manifested as differences in ENSO decay rate and spatial structure, together with the state of spring TNA SST, may play important roles in distinguishing North American spring temperature evolutions.

3.3 The Atlantic pathway

Some recent studies have suggested that TNA SST can shape North American spring mean temperature anomalies, primarily through its influence on the North Atlantic circulation patterns (Fu et al., 2025; Hou et al., 2023; Ji et al., 2025). Here, we further examine the linkage between TNA SST and month-to-month temperature evolutions over North America (Fig. 6a–c). The TNA-related SAT anomaly patterns closely resemble those of S-EOF1, with pattern correlation coefficients of 0.90, 0.78, and 0.54 for March, April, and May, respectively. Circulation anomalies over the North Atlantic exhibit a negative NAO-like pattern, although the southern center weakens or becomes absent in May (Fig. 6a–c), consistent with a less coherent temperature dipole over North America during that month. Generally, spring TNA SST anomalies tend to favor a persistent north–south temperature dipole over North America, similar to S-EOF1. These results are supportive of previous studies focusing on the seasonal mean state (Fu et al., 2025; Hou et al., 2023; Ji et al., 2025), as S-EOF1 represents a persistent temperature mode with relatively weak subseasonal variation.

It has been acknowledged that tropical Pacific SST anomalies in winter can influence spring TNA SST through a Gill-type atmospheric response, which suppresses precipitation over the tropical Atlantic and weakens low-level convergence and trade winds (Chen et al., 2021; Xie and Carton, 2004; Zhang and Jiang, 2023). However, both S-EOF modes are preceded by Pacific SST warming, raising the question of why they exhibit distinct linkages with spring TNA SST (Fig. 7a, b). Interestingly, the two S-EOF modes correspond to opposite phases of the NAO in early spring (March; Fig. 3b,

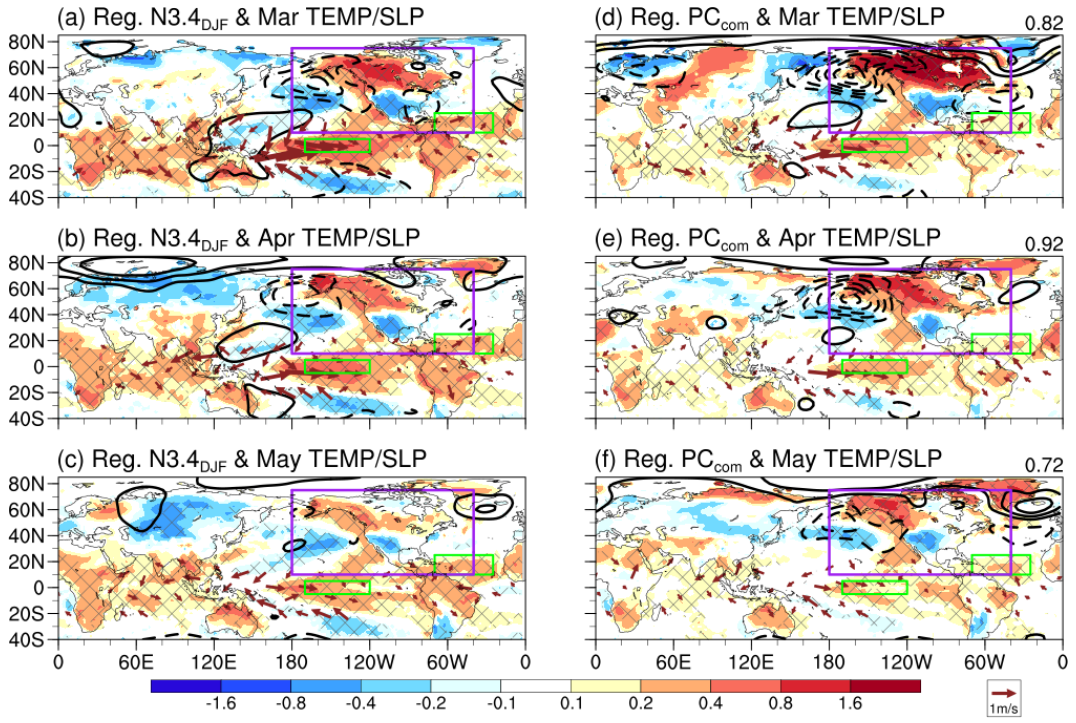


Figure 5. (a–c) Temperature anomalies (shading; unit: °C per standard deviation of the regressed index; with SST over ocean and SAT over land), SLP anomalies (black contours; unit: hPa per standard deviation of the regressed index; 0.5 hPa interval with zero contour omitted), and 925 hPa wind anomalies (vectors; unit: m s^{-1} per standard deviation of the regressed index; vectors plotted only in the tropics) in **(a)** March, **(b)** April, and **(c)** May regressed onto the standardized winter Niño3.4 index. All fields are linearly detrended prior to regression. Cross-hatching indicates regions where the regressed temperature anomalies are significant at the 95% confidence level based on a two-tailed Student's t test. Green boxes over the Pacific and Atlantic Oceans denote the Niño3.4 and TNA regions, respectively. The purple box outlines North America. **(d–f)** Same as **(a–c),** but for anomalies regressed onto the standardized PC combination index (defined as the sum of PC1 and PC2). Numbers in the top-right corner of each panel indicate the pattern correlation coefficients between North American SAT anomalies regressed onto the standardized PC combination index and those regressed onto the standardized winter Niño3.4 index.

f; Table 1), which has also been identified as a key regulator of TNA SST (Chen et al., 2021; Xie and Carton, 2004; Zhang and Jiang, 2023). This suggests that phase changes of the early spring NAO may play a crucial role in modulating TNA SST responses to tropical Pacific warming.

To further quantify these effects, we decompose the spring TNA SST index into two components (Fig. 7c): an ENSO-related component derived from the linear regression of spring TNA SST onto the winter Niño3.4 index, and a non-ENSO component defined as the residual. The non-ENSO component is comparable to, and can even exceed, the ENSO-related component in magnitude. Moreover, the early spring NAO is significantly correlated with the non-ENSO component ($r = -0.37$), but only weakly correlated with the ENSO-related component ($r = 0.11$). These results suggest that early spring NAO is largely independent of winter ENSO and can exert a significant impact on spring TNA SST.

The probability density functions (PDFs) of the spring TNA SST index and its two components under different combinations of ENSO and NAO phases are shown in Fig. 7d–g. During El Niño years, the ENSO-related component exhibits relatively consistent behavior regardless of the early spring NAO phase, whereas the non-ENSO component varies markedly (Fig. 7d, e). Notably, the non-ENSO component exhibits a larger spread than the ENSO-related component, likely reflecting greater uncertainty in local air–sea interactions (Xie and Carton, 2004), potentially amplified by early spring NAO.

During the negative phase of early spring NAO, a weakened subtropical high and reduced trade winds favor warmer TNA SST that tends to persist throughout spring (Chen et al., 2021; Xie and Carton, 2004; Zhang and Jiang, 2023), whereas the opposite occurs during the positive phase (Fig. 6d–f). Consequently, the early spring NAO can either reinforce or offset the influence of winter ENSO: negative NAO phases amplify ENSO-induced TNA warming (Fig. 7d), whereas positive NAO phases suppress it (Fig. 7e). Similar behavior is found during La Niña years (Fig. 7f, g). These results suggest a "tug-of-war" over the TNA region, in which the ENSO-driven SST signal is strongly modulated by the phase of the early spring NAO. This interplay

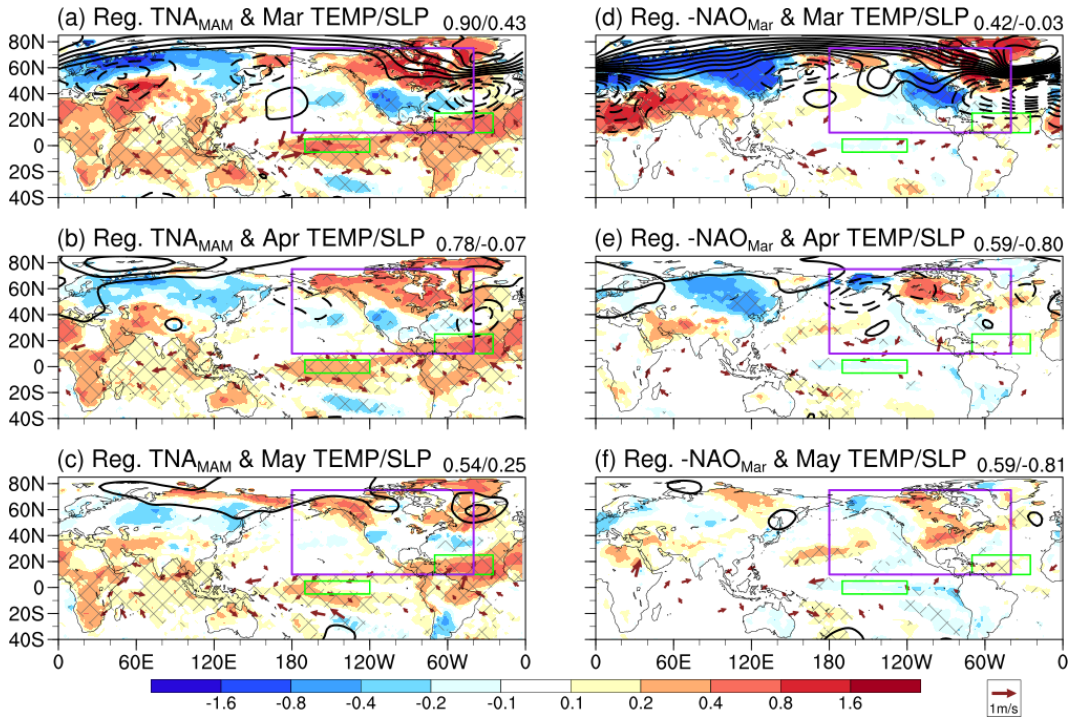


Figure 6. (a–c) Temperature anomalies (shading; unit: °C per standard deviation of the regressed index; with SST over ocean and SAT over land), SLP anomalies (black contours; unit: hPa per standard deviation of the regressed index; 0.5 hPa interval with zero contour omitted), and 925 hPa wind anomalies (vectors; unit: m s^{-1} per standard deviation of the regressed index; vectors plotted only in the tropics) in **(a)** March, **(b)** April, and **(c)** May regressed onto the standardized spring TNA index. All fields are linearly detrended prior to regression. Cross-hatching indicates regions where the regressed temperature anomalies are significant at the 95 % confidence level based on a two-tailed Student's *t* test. Green boxes over the Pacific and Atlantic Oceans denote the Niño3.4 and TNA regions, respectively. The purple box outlines North America. Numbers in the top-right corner of each panel indicate the pattern correlation coefficients between North American SAT anomalies regressed onto the standardized spring TNA index and those regressed onto the standardized PC1/PC2. **(d–f)** Same as **(a–c)**,but for anomalies regressed onto the standardized early spring negative NAO index (for better comparison with the spring TNA). Numbers in the top-right corner of each panel indicate the pattern correlation coefficients between North American SAT anomalies regressed onto the standardized early spring negative NAO index and those regressed onto the standardized PC1/PC2.

is closely linked to the two S-EOF modes. A negative relationship between winter ENSO and the early spring NAO, associated with S-EOF1, tends to promote the development of pronounced TNA SST anomalies in spring, whereas a positive relationship, associated with S-EOF2, tends to suppress their development (Fig. 3). The resulting TNA SST state—whether anomalies are present or absent – helps distinguish between persistent and evolving North American temperature patterns (Fig. 6a–c) through its linkage with North Atlantic circulation (Fu et al., 2025; Hou et al., 2023; Ji et al., 2025).

3.4 The Pacific pathway

The above discussion focuses on the Atlantic sector associated with the two S-EOF modes, in which the ENSO–TNA linkage and the influence of the early spring NAO play important but distinct roles. We now turn to the Pacific sector to examine the midlatitude circulation patterns associated with the S-EOF modes and their potential linkages with tropical Pacific SST anomalies. Here, S-EOF1 is primarily linked to the spring NPO (i.e., North Pacific Oscillation, $r = 0.62$), while S-EOF2 is closely related to the spring NP (i.e., North Pacific, $r = 0.59$).

The NPO is characterized by a north–south SLP dipole over the North Pacific (Fig. 8a–c), with its northern center extending from the Bering Strait toward North America. In particular, the anomalous low to the north occupies much of the North American continent, inducing southeasterly wind anomalies over central–eastern North America. In contrast, the southwestern United States lies between the eastern flank of the anomalous high over the subtropical North Pacific and the western edge of the anomalous low over North America. The resulting northerly wind anomalies primarily enhance regional cooling. Therefore, the circulation pattern associated with the NPO favors a north–south temperature dipole over North America. Moreover, the NPO pattern remains relatively stable throughout the spring, thereby maintaining persistent temperature anomalies over North America (Fig. 8a–

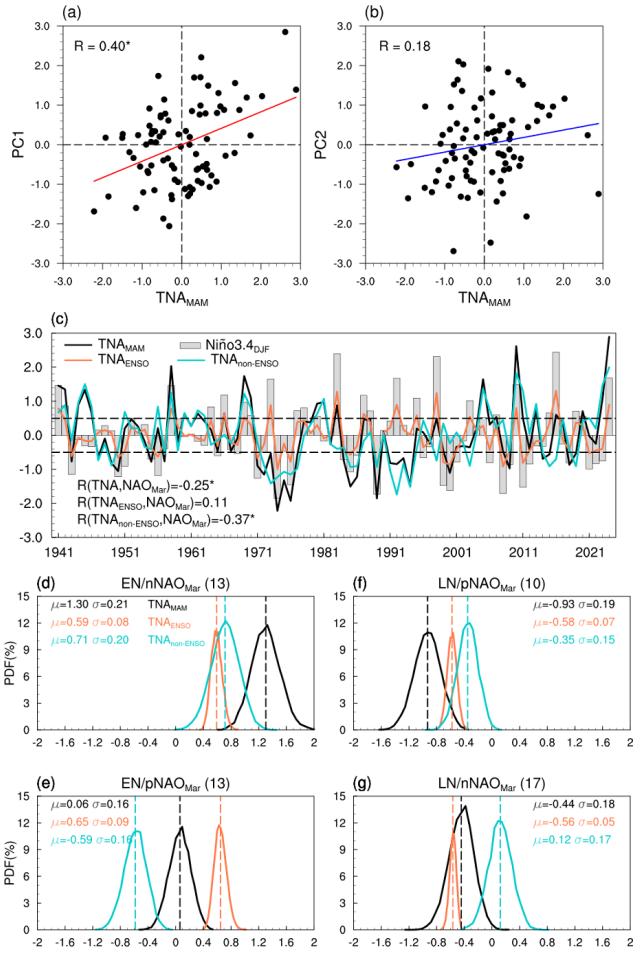


Figure 7. (a–b) Scatterplots of the standardized spring TNA SST index versus **(a)** the standardized PC1 and **(b)** the standardized PC2. Red and blue lines denote linear regression fits, with corresponding correlation coefficients shown in the top-left of each panel. **(c)** Standardized time series of the spring TNA SST index (black line), its ENSO-related component (orange line), its non-ENSO component (cyan line), and the standardized winter Niño3.4 index (bars). Horizontal dashed lines denote ±0.5 standard deviations. Numbers in the bottom-left indicate the correlation coefficients between the spring TNA SST index, its two components, and the early spring NAO. **(d–g)** Probability density functions (PDFs; unit: %) of the standardized spring TNA SST index (black line), its ENSO-related component (orange line), and its non-ENSO component (cyan line) under different combinations of winter ENSO and early spring NAO: **(d)** El Niño with negative NAO (13 samples), **(e)** El Niño with positive NAO (13 samples), **(f)** La Niña with positive NAO (10 samples), and **(g)** La Niña with negative NAO (17 samples). PDFs are estimated using a bootstrap method with 10 000 resamples. El Niño (La Niña) events are defined when the standardized winter Niño3.4 index is greater than (lower than) 0.5 (−0.5) standard deviation. A positive (negative) NAO is defined when the early spring NAO index exceeds (falls below) 0. Mean values and standard deviations of the spring TNA SST index and its two components are shown at the top of each panel.

c). The SAT anomalies associated with the spring NPO are highly consistent with those of S-EOF1, with pattern correlation coefficients of 0.93, 0.98, and 0.93 for March, April, and May, respectively. The NPO appears largely independent of conventional ENSO, as indicated by its weak correlation with the Niño3.4 index in both winter and spring (Table 1). Consistently, the NPO-related temperature pattern remains largely unchanged after removing signals related to the Niño3.4 index in both seasons (Fig. S1 in the Supplement). These results suggest that, as tropical Pacific SST anomalies decay from winter to spring (Fig. 4a), the NPO and its influence on North American spring temperature become more prominent and operate with limited modulation by conventional ENSO-driven North Pacific circulation anomalies. Interestingly, the spring NPO is significantly correlated with the EPI, but not with the CPI (Table 1), suggesting a preferential linkage between EP ENSO and the NPO. However, this does not necessarily indicate that the relationship between EP ENSO and S-EOF1 is mediated by the spring NPO, because the EPI–NPO correlation is no longer significant after excluding years with extreme EPI values exceeding 4 standard deviations (Table S1). Therefore, the apparent preferential linkage between EP ENSO and the NPO does not appear to be a robust relationship, but is instead largely dependent on a few extreme EP ENSO years. Although a potential role of EP ENSO cannot be ruled out, this apparent linkage should be interpreted with caution. Apart from tropical Pacific SST anomalies, the spring IOD is also significantly correlated with the spring NPO (Table 1). While this simultaneous relationship does not imply causality, previous studies have shown that Indian Ocean variability can modulate tropical Pacific SST evolution through subtropical Pacific processes in which the NPO also plays an important role (Lin and Yu, 2024). This suggests that the co-variability between the IOD and NPO may provide a potential pathway linking Indian Ocean variability to S-EOF1, although the underlying physical mechanisms require further investigation.

Circulation anomalies associated with the spring NP index manifest as a large-scale low-pressure system over the North Pacific (Fig. 8d–f). Compared to the NPO (Fig. 8a–c), the loading center of this anomalous low is located farther south, near the Aleutian Islands, and is primarily confined to the ocean, with limited extension toward North America. In addition, pronounced month-to-month variations are evident from March to May (Fig. 8d–f). This anomalous low extends southeastward, accompanied by the development of an anomalous high over the North American Arctic in April and May. These circulation changes closely resemble those related to S-EOF2 (Fig. 3f–h). Note that the spring NP index is significantly correlated with the Niño3.4 index in spring, but not in winter (Table 1). The SAT anomaly patterns associated with the spring NP index remain similar, albeit weaker, after removing the influence of the spring Niño3.4 index, compared to those obtained after removing the winter Niño3.4 index (Fig. S2). These results suggest that stronger tropical

Pacific SST anomalies in spring may enhance the anomalous low over the North Pacific and promote the evolving temperature patterns over North America. This is consistent with the finding that S-EOF2 is associated with more persistent tropical Pacific SST anomalies from winter to spring (Fig. 4b). We also find a modest linkage between CP ENSO and the NP pattern (Table 1), raising the possibility that the influence of CP ENSO on North American spring temperature anomalies may be partly mediated through its connection with the NP pattern. However, it is difficult to determine whether this linkage primarily reflects differences in ENSO decay rate, spatial structure, or a combination of both, because CP ENSO itself tends to exhibit greater persistence into spring (Kao and Yu, 2009; Lee et al., 2014; Ren et al., 2016).

These results based on the spring-mean NPO and NP indices are generally consistent with those based on the monthly indices (not shown), indicating that the monthly evolution of the NPO (NP)-related circulation corresponds to the persistent (evolving) temperature pattern associated with S-EOF1 (S-EOF2).

3.5 Relative contributions of tropical SST and midlatitude circulation

To further quantify the relative contributions of different tropical SST and midlatitude circulation patterns in influencing the two S-EOF modes, we adopt a dominance analysis (Azen and Budescu, 2003; Grömping, 2007) to partition the explained variance among correlated climate indices across all possible regression model orderings (Fig. 9). Six climate indices (i.e., the winter EPI (for PC1)/CPI (for PC2), the spring TNA index, the spring IOD index, the spring NPO index, the spring NP index, and the early spring NAO index) are selected based on the physical mechanisms discussed above. Note that the selection of EPI for PC1 and CPI for PC2 is based on their respective significant correlations with PC1 and PC2, whereas the cross-correlations (CPI with PC1 and EPI with PC2) are not statistically significant.

The regression coefficient heatmaps for all subset models indicate that S-EOF1 is primarily dominated by the spring NPO index, as evidenced by its consistently large coefficients across models (Fig. 9a). This dominance is further supported by its contribution to explained variance, accounting for 26.7 % on average, with well-separated bootstrap uncertainty ranges of the averaged explained variance before and after its inclusion (Fig. 9c). The spring TNA index provides the second-largest contribution (10.4 %; Fig. 9c), further supporting an important role of the Atlantic pathway in shaping S-EOF1. The winter EPI, spring IOD index and spring NP index are also positively related to PC1, but their contributions are comparatively smaller (5.4 %, 3.5 %, and 2.6 %, respectively; Fig. 9c). Notably, the regression coefficients of the early spring NAO are consistently negative across all models (Fig. 9a), indicating a robust and independent negative relationship with the PC1, with minimal evidence of competing effects from other variables. The early spring NAO contributes 3.0 % to the PC1 (Fig. 9c). More than half of the variance of PC1 (51.6 %) is explained by these six climate indices (Fig. 9c).

In contrast, S-EOF2 is primarily influenced by the spring NP index, which exhibits the strongest and most consistent contributions across models (Fig. 9b), accounting for 32.9 % of the explained variance (Fig. 9d). The bootstrap results confirm the robust contribution of the spring NP index to S-EOF2. The winter CPI makes a substantial contribution of 12.3 % (Fig. 9d), providing additional evidence for a preferential linkage between CP ENSO and S-EOF2. The early spring NAO index, spring NPO index, and spring IOD index contribute 4.9 %, 3.9 %, and 1.2 %, respectively (Fig. 9d). The regression coefficients of the spring TNA index, however, vary substantially, particularly in models that include the winter CPI, suggesting a competing or modulated role (Fig. 9b). This behavior supports the earlier inference that, for S-EOF2, the ENSO–TNA linkage may be weakened or overridden by other factors, like the early spring NAO. Consistent with this, the spring TNA index contributes only 2.0 % (Fig. 9d). These six climate indices explain 57.3 % of the total variance of PC2 (Fig. 9d), slightly higher than that for PC1 (51.6 %). The generally smaller bootstrap uncertainty ranges of the complete model for PC2 than for PC1 suggest that S-EOF2 may be more strongly constrained by these climate drivers.

4 Conclusions and discussion

This study identifies two leading modes of North American spring temperature evolution that differ from conventional ENSO responses and are linked to distinct tropical SST regimes and midlatitude circulation. Differences in ENSO decay rate, spatial structure, and the state of TNA SST help distinguish the two modes. A fast-decaying EP ENSO-like SST pattern favors the development of spring TNA SST anomalies, which, together with the NPO, promote a persistent north–south temperature dipole over North America (i.e., S-EOF1). In contrast, a more persistent CP ENSO-like pattern into spring enhances the role of the NP pattern in shaping an evolving temperature pattern over North America (i.e., S-EOF2). The absence of spring TNA SST anomalies in association with S-EOF2 is likely due to an offsetting effect of the early spring NAO.

The results suggest two distinct dynamical pathways linking tropical SST variability to North American spring temperatures. The first is an Atlantic pathway, in which winter ENSO influences spring TNA SST through a delayed response (Chen et al., 2021). The resulting TNA SST anomalies further interact with the early spring NAO, modulating North Atlantic circulation and thereby reinforcing or weakening temperature persistence over North America. The sec-

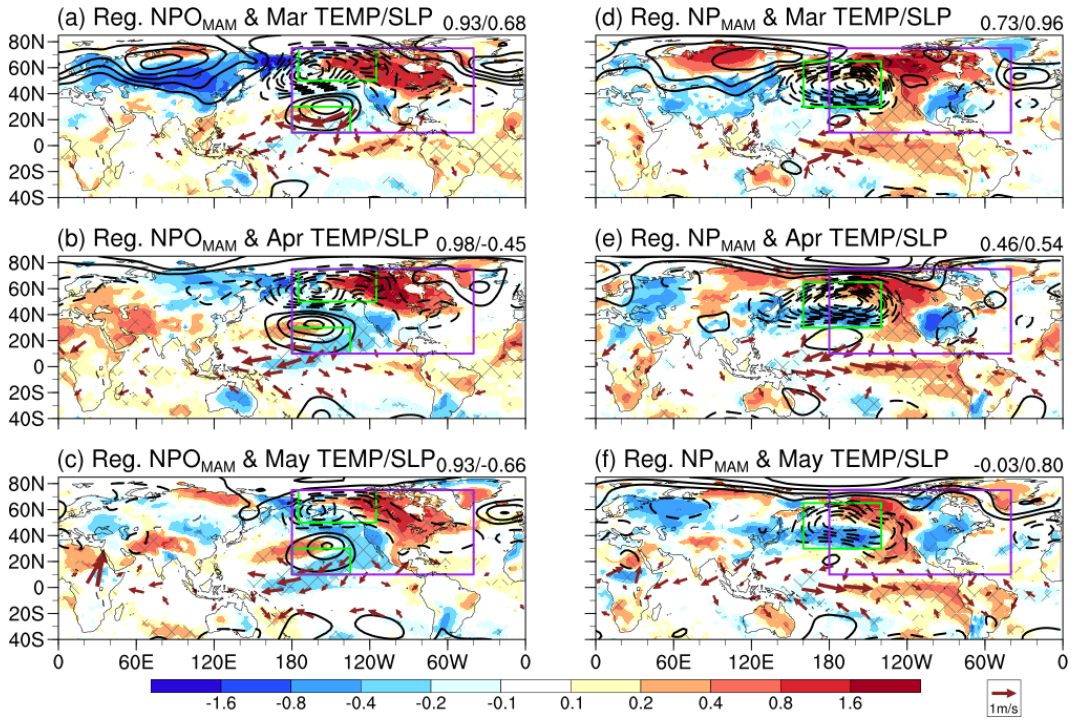


Figure 8. (a–c) Temperature anomalies (shading; unit: °C per standard deviation of the regressed index; with SST over ocean and SAT over land), SLP anomalies (black contours; unit: hPa per standard deviation of the regressed index; 0.5 hPa interval with zero contour omitted), and 925 hPa wind anomalies (vectors; unit: m s^{-1} per standard deviation of the regressed index; vectors plotted only in the tropics) in **(a)** March, **(b)** April, and **(c)** May regressed onto the standardized spring NPO index. All fields are linearly detrended prior to regression. Cross-hatching indicates regions where the regressed temperature anomalies are significant at the 95 % confidence level based on a two-tailed Student's *t* test. Green boxes over the North Pacific denote the key regions used to define the NPO. The purple box outlines North America. Numbers in the top-right corner of each panel indicate the pattern correlation coefficients between North American SAT anomalies regressed onto the standardized spring NPO index and those regressed onto the standardized PC1/PC2. **(d–f)** Same as **(a–c)**, but for anomalies regressed onto the standardized spring NP index. The green box over the North Pacific denotes the key region used to define the NP. Numbers in the top-right corner of each panel indicate the pattern correlation coefficients between North American SAT anomalies regressed onto the standardized spring NP index and those regressed onto the standardized PC1/PC2.

ond is a Pacific pathway, in which persistent CP ENSO-like SST anomalies more directly modulate the NP pattern, whereas less persistent EP ENSO-like SST anomalies may provide favorable conditions for the development of the NPO pattern. These contrasting pathways highlight the role of tropical SST regimes in shaping distinct midlatitude circulation patterns and associated temperature responses over North America.

By applying the dominance analysis, we quantitatively assess the relative importance of tropical SST and midlatitude circulation patterns in shaping the two modes. This approach provides a more robust attribution framework in the presence of correlated climate indices, highlighting the dominant role of the NPO pattern in S-EOF1 and the NP pattern in S-EOF2, while also clarifying the modulated contributions of ENSO and TNA SST.

Our findings are consistent with previous studies highlighting the role of tropical Atlantic SST in modulating North American spring climate (Fu et al., 2025; Hou et al., 2023; Ji et al., 2025), while extending their results by demonstrating that the emergence of TNA SST anomalies and their impacts on the midlatitudes can be jointly influenced by ENSO and early spring NAO. Despite the important connection between the early spring NAO and the contrasting evolution of TNA SST anomalies following winter ENSO, as discussed in this study and also suggested by previous work (Chen et al., 2021; Ding et al., 2023; Tian et al., 2025; Xie and Carton, 2004; Zhang and Jiang, 2023), the physical origin of the opposite NAO phases remains unclear and warrants further investigation. No significant relationship is detected between the early spring NAO and either ENSO or the IOD, suggesting that the occurrence of opposite NAO phases is not closely associated with differences in these tropical SST forcings and may instead reflect, at least in part, internal atmospheric variability.

In addition, this study complements earlier work on ENSO diversity by showing that differences in ENSO seasonal evolution and flavor may correspond to distinct extratropical re-

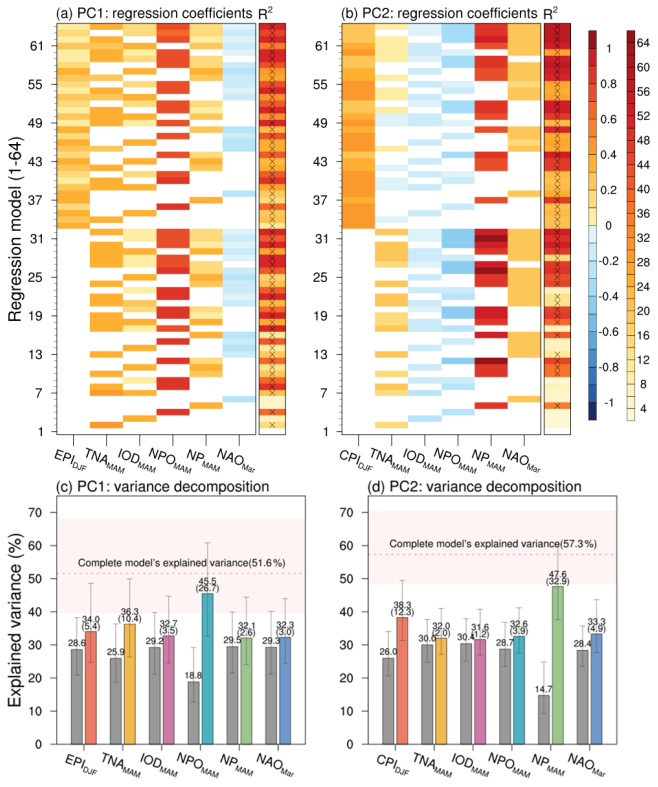


Figure 9. (a–b) Heatmaps of regression coefficients (first six columns) and explained variance (R^2, seventh column, unit: %) for all subset regression models of **(a)** PC1 and **(b)** PC2, constructed from different combinations of the winter EPI (for PC1)/CPI (for PC2), the spring TNA index, the spring IOD index, the spring NPO index, the spring NP index, and the early spring NAO index. All indices are standardized and linearly detrended. Model 1 corresponds to the null model (no variables) and is included as a baseline. The cross marks in the seventh column indicate that the corresponding regression models are statistically significant at the 95 % confidence level based on a two-tailed Student's t test. **(c–d)** Variance decomposition (dominance analysis) for **(c)** PC1 and **(d)** PC2, using the winter EPI (for PC1)/CPI (for PC2), the spring TNA index, the spring IOD index, the spring NPO index, the spring NP index, and the early spring NAO index. Gray bars denote the weighted-average R^2 of models excluding a given variable (32 combinations), while colored bars denote the weighted-average R^2 after including that variable (another 32 combinations). Values above the gray (colored) bars indicate the R^2 before (after) including each variable, with the corresponding incremental contributions shown in parentheses above the colored bars. Error bars on the gray and colored bars indicate the 5th and 95th percentiles of the bootstrap distributions based on 10 000 resamples of years. The red dashed line represents the R^2 of the complete model (Model 64), corresponding to the sum of the contributions from all individual variables, and the red shading indicates its 5th–95th percentile bootstrap range. See Methods for details of the dominance analysis and bootstrap procedure.

sponses (Jong et al., 2020). The NPO- and NP-related circulation patterns are likely to connect with differences in ENSO decay rate and spatial structure (Fig. 8), further emphasizing the combined influence of tropical forcing and internal atmospheric variability on North American spring climate. However, the relative roles of ENSO decay rate and spatial structure in shaping these contrasting extratropical responses remain difficult to disentangle, particularly because EP and CP ENSO tend to exhibit different decay rates (Kao and Yu, 2009; Lee et al., 2014; Ren et al., 2016).

It is also interesting to note that Eurasian temperature anomalies exhibit distinct subseasonal evolution in association with these two S-EOF modes (Fig. 3). These features are particularly pronounced in March (Fig. 3b, f), when the two modes are accompanied by opposite phases of the NAO and contrasting temperature anomalies over Eurasia, followed by distinct evolutions in April and May (Fig. 3c–d, g–h). The co-occurrence of temperature anomalies over the two continents is consistent with large-scale atmospheric variability, particularly the NAO. As this study mainly focuses on North American spring temperature evolution, a detailed investigation of the Eurasian temperature anomalies and their underlying mechanisms is beyond the scope of this study.

We have also examined the evolution of snowfall, surface albedo, and soil moisture anomalies associated with the two S-EOF modes (not shown). S-EOF1 is associated with snowfall anomalies over western Canada in the preceding winter, followed by persistent surface albedo anomalies during spring, suggesting a potential positive snow–albedo feedback that may contribute to the persistence of the temperature pattern. In contrast, S-EOF2 shows no obvious snowfall anomalies in the preceding winter. Neither mode exhibits significant linkages with preceding soil moisture anomalies, while simultaneous soil moisture anomalies show a less coherent relationship with the temperature evolution, likely reflecting the influence of other physical processes.

These findings have important implications for seasonal prediction. Accurately representing ENSO decay rate, spatial structure, and TNA SST variability may improve predictions of North American spring temperature evolution. Furthermore, the interplay between tropical SST and midlatitude atmospheric variability suggests that incorporating both sources of predictability is essential for improving subseasonal-to-seasonal forecasts. Future work should explore the representation of these processes in climate models, their sensitivity to model biases, and their potential changes in a warming climate.

Code and data availability. The ECMWF ERA5 reanalysis data and the NOAA ERSST v5 data are publicly available from the following websites: https://cds.climate.copernicus.eu/ (last access: 15 September 2026), https://psl.noaa.gov/data/gridded/data.noaa.ersst.v5.html (last access: 15 September 2026), respectively. The Niño3.4 index, the IOD index, the NP index, and the NAO index

are available from the following websites: https://psl.noaa.gov/data/timeseries/month/DS/Nino34/ (last access: 15 September 2026), https://psl.noaa.gov/data/timeseries/month/DMI/ (last access: 15 September 2026), https://climatedataguide.ucar.edu/climate-data/north-pacific-np-index-trenberth-and-hurrell-monthly-and-winter, https://crudata.uea.ac.uk/cru/data/nao/ (last access: 15 September 2026), respectively. Other data used in this study can be obtained from the first author upon request.

All figures in this paper are produced by NCAR Command Language (NCL) version 6.5.0. Source codes are available upon reasonable request to the first author.

Supplement. The supplement related to this article is available online at https://doi.org/10.5194/wcd-7-2251-2026-supplement.

Author contributions. WGZ and MFT designed the research and prepared the manuscript. WGZ collected the data, conducted the analysis, and produced all figures. WGZ, MFT, and ZWW discussed the results, reviewed the manuscript, and improved the presentation.

Competing interests. The contact author has declared that none of the authors has any competing interests.

Disclaimer. Publisher's note: Copernicus Publications remains neutral with regard to jurisdictional claims made in the text, published maps, institutional affiliations, or any other geographical representation in this paper. The authors bear the ultimate responsibility for providing appropriate place names. Views expressed in the text are those of the authors and do not necessarily reflect the views of the publisher.

Acknowledgements. We thank Drs. Clara Deser (NCAR), Bin Wang (University of Hawaii), and Yutian Wu (Columbia University) for helpful discussions.

Financial support. Wogu Zhong is supported by the National Natural Science Foundation of China (NSFC) (grant no. 42505017). Zhiwei Wu is supported by the Ministry of Science and Technology of China (grant no. 2023YFF0805100).

Review statement. This paper was edited by Gwendal Rivière and reviewed by two anonymous referees.

References

Abatzoglou, J. T. and Redmond, K. T.: Asymmetry between trends in spring and autumn temperature and circulation regimes over western North America, Geophys. Res. Lett., 34, L18808, https://doi.org/10.1029/2007gl030891, 2007.

Ault, T. R., Macalady, A. K., Pederson, G. T., Betancourt, J. L., and Schwartz, M. D.: Northern Hemisphere Modes of Variability and the Timing of Spring in Western North America, J. Clim., 24, 4003–4014, https://doi.org/10.1175/2011jcli4069.1, 2011.

Azen, R. and Budescu, D. V.: The dominance analysis approach for comparing predictors in multiple regression, Psychol. Methods, 8, 129–148, https://doi.org/10.1037/1082-989X.8.2.129, 2003.

Barcikowska, M. J., Muñoz, Á. G., Weaver, S. J., Russo, S., and Wehner, M.: On the potential impact of a half-degree warming on cold and warm temperature extremes in mid-latitude North America, Environ. Res. Lett., 14, 124040, https://doi.org/10.1088/1748-9326/ab4dea, 2019.

Breeden, M. L., Albers, J. R., Butler, A. H., and Newman, M.: The Spring Minimum in Subseasonal 2-m Temperature Forecast Skill over North America, J. Clim., 150, 2617–2628, https://doi.org/10.1175/MWR-D-22-0062.1, 2022.

Byrne, B., Liu, J., Bloom, A. A., Bowman, K. W., Butterfield, Z., Joiner, J., Keenan, T. F., Keppel-Aleks, G., Parazoo, N. C., and Yin, Y.: Contrasting Regional Carbon Cycle Responses to Seasonal Climate Anomalies Across the East-West Divide of Temperate North America, Global Biogeochem. Cy., 34, e2020GB006598, https://doi.org/10.1029/2020GB006598, 2020.

Chamberlain, C. J., Cook, B. I., García de Cortázar-Atauri, I., and Wolkovich, E. M.: Rethinking false spring risk, Global Chang. Biol., 25, 2209–2220, https://doi.org/10.1111/gcb.14642, 2019.

Chen, H., Jin, F., and Jiang, L.-S.: The Phase-Locking of Tropical North Atlantic and the Contribution of ENSO, Geophys. Res. Lett., 48, e2021GL095610, https://doi.org/10.1029/2021GL095610, 2021.

Chen, R. Y., Simpson, I. R., Deser, C., and Wang, B.: Model Biases in the Simulation of the Springtime North Pacific ENSO Teleconnection, J. Clim., 33, 9985–10002, https://doi.org/10.1175/JCLI-D-19-1004.1, 2020.

Choi, W. and Kim, K.-Y.: Physical mechanism of spring and early summer drought over North America associated with the boreal warming, Sci. Rep., 8, 7533, https://doi.org/10.1038/s41598-018-25932-5, 2018.

Ding, R., Nnamchi, H. C., Yu, J.-Y., Li, T., Sun, C., Li, J., Tseng, Y., Li, X., Xie, F., Feng, J., Ji, K., and Li, X.: North Atlantic oscillation controls multidecadal changes in the North Tropical Atlantic−Pacific connection, Nat. Commun., 14, 862, https://doi.org/10.1038/s41467-023-36564-3, 2023.

Ding, X. Y., Chen, G., Wang, Y., and Sun, L. T.: Demystifying the drivers of the spring warming asymmetry between Eurasia and North America, Sci. Adv., 11, eadu2364, https://doi.org/10.1126/sciadv.adu2364, 2025.

Diro, G. T., Sushama, L., and Huziy, O.: Snow-atmosphere coupling and its impact on temperature variability and extremes over North America, Clim. Dynam., 50, 2993–3007, https://doi.org/10.1007/s00382-017-3788-5, 2018.

Fragkoulidis, G., Wirth, V., Bossmann, P., and Fink, A. H.: Linking Northern Hemisphere temperature extremes to Rossby wave packets, Q. J. Roy. Meteorol. Soc., 144, 553–566, https://doi.org/10.1002/qj.3228, 2018.

Fu, S. S., Zhu, Z. W., Yu, H. P., and Li, T.: The diversity of the boreal spring North Atlantic sea surface temperature tripole pattern and corresponding Northern Hemispheric sur-

face air temperature anomalies, Environ. Res. Lett., 20, 054043, https://doi.org/10.1088/1748-9326/adca47, 2025.

Geng, T., Cai, W. J., Wu, L. X., Santoso, A., Wang, G., Jing, Z., Gan, B. L., Yang, Y., Li, S. J., Wang, S. P., Chen, Z. H., and McPhaden, M. J.: Emergence of changing Central-Pacific and Eastern-Pacific El Niño-Southern Oscillation in a warming climate, Nat. Commun., 13, 6616, https://doi.org/10.1038/s41467-022-33930-5, 2022.

Grömping, U.: Estimators of Relative Importance in Linear Regression Based on Variance Decomposition, Am. Stat., 61, 139–147, https://doi.org/10.1198/000313007X188252, 2007.

He, B. and Yang, S.: Role of Latent Heating over the Tropical Western Pacific in Surface Temperature Change over North America during Boreal Spring, J. Clim., 31, 2169–2184, https://doi.org/10.1175/JCLI-D-17-0388.1, 2018.

Hersbach, H., Bell, B., Berrisford, P., Hirahara, S., Horányi, A., Muñoz-Sabater, J., Nicolas, J., Peubey, C., Radu, R., Schepers, D., Simmons, A., Soci, C., Abdalla, S., Abellan, X., Balsamo, G., Bechtold, P., Biavati, G., Bidlot, J., Bonavita, M., Chiara, G., Dahlgren, P., Dee, D., Diamantakis, M., Dragani, R., Flemming, J., Forbes, R., Fuentes, M., Geer, A., Haimberger, L., Healy, S., Hogan, R. J., Hólm, E., Janisková, M., Keeley, S., Laloyaux, P., Lopez, P., Lupu, C., Radnoti, G., Rosnay, P., Rozum, I., Vamborg, F., Villaume, S., and Thépaut, J.: The ERA5 global reanalysis, Q. J. Roy. Meteorol. Soc., 146, 1999–2049, https://doi.org/10.1002/qj.3803, 2020.

Hou, Y. R., Johnson, N. C., Chang, C., Sun, W. J., Man, K., Miao, Y. J., and Li, X. C.: Cold Springs Over Mid-Latitude North America Induced by Tropical Atlantic Warming, Geophys. Res. Lett., 50, e2023GL104180, https://doi.org/10.1029/2023GL104180, 2023.

Hu, S. Q., Watanabe, M., Zhang, W. J., Iwakiri, T., and Jiang, F.: Quantifying the Amplifying Effect of the Winter North Pacific Oscillation on the Subsequent ENSO, Geophys. Res. Lett., 51, e2024GL111019, https://doi.org/10.1029/2024GL111019, 2024.

Huang, B. Y., Thorne, P. W., Banzon, V. F., Boyer, T., Chepurin, G., Lawrimore, J. H., Menne, M. J., Smith, T. M., Vose, R. S., and Zhang, H.-M.: Extended reconstructed sea surface temperature, version 5 (ERSST v5): upgrades, validations, and intercomparisons, J. Clim., 30, 8179–8205, https://doi.org/10.1175/JCLI-D-16-0836.1, 2017.

Hurrell, J. W.: Decadal trends in the North Atlantic Oscillation: regional temperatures and precipitation, Science, 269, 676–679, 1995.

Hwang, J., You, Z. Y., He, J., and Deng, Y.: Dynamics and model representation of the boreal spring subseasonal variability over North America, Clim. Dynam., 63, 360, https://doi.org/10.1007/s00382-025-07859-6, 2025.

Ji, K. and Ding, R. Q.: Interannual impact of the Victoria mode on the winter-spring surface air temperature over Eurasia and North America, npj Clim. Atmos. Sci., 6, 114, https://doi.org/10.1038/s41612-023-00440-0, 2023.

Ji, K., Ding, R. Q., Zheng, J. Y., and Qian, Q. F.: Nonstationary modulation of the preceding spring North Pacific Victoria mode on the connection of central North America winter temperature with ENSO, Clim. Dynam., 62, 37–53, https://doi.org/10.1007/s00382-023-06895-4, 2024.

Ji, K., Ding, R. Q., and Mei, L. L.: The synergistic effect of the North Pacific and the North Tropical Atlantic sea surface temperature on winter–spring cold events in Eastern North America, npj Clim. Atmos. Sci., 8, 189, https://doi.org/10.1038/s41612-024-00892-y, 2025.

Jones, P. D., Jonsson, T., and Wheeler, D.: Extension to the North Atlantic oscillation using early instrumental pressure observations from Gibraltar and south-west Iceland, Int. J. Climatol., 17, 1433–1450, 1997.

Jong, B.-T., Ting, M. F., Seager, R., and Anderson, W. B.: ENSO Teleconnections and Impacts on U.S. Summertime Temperature during a Multiyear La Niña Life Cycle, J. Clim., 33, 6009–6024, https://doi.org/10.1175/jcli-d-19-0701.1, 2020.

Kao, H.-Y. and Yu, J.-Y.: Contrasting Eastern-Pacific and Central-Pacific Types of ENSO, J. Clim., 22, 615–632, https://doi.org/10.1175/2008JCLI2309.1, 2009.

Leduc, M. and Logan, T.: The Impact of Climate Change on the Annual Cycle of Freeze–Thaw Events in Eastern North America, J. Appl. Meteorol. Climatol., 64, 1323–1341, https://doi.org/10.1175/JAMC-D-24-0190.1, 2025.

Lee, S., Mapes, B. E., Wang, C., Enfield, D. B., and Weaver, S. J.: Springtime ENSO phase evolution and its relation to rainfall in the continental U.S., Geophys. Res. Lett., 41, 1673–1680, https://doi.org/10.1002/2013GL059137, 2014.

Lin, Y.-F. and Yu, J.-Y.: The Role of the Indian Ocean in Controlling the Formation of Multiyear El Niños through Subtropical ENSO Dynamics, J. Clim., 37, 385–401, https://doi.org/10.1175/JCLI-D-23-0297.1, 2024.

McDonald, K. W., McClure, C. J. W., Rolek, B. W., and Hill, G. E.: Diversity of birds in eastern North America shifts north with global warming, Ecol. Evol., 2, 3052–3060, https://doi.org/10.1002/ece3.410, 2012.

Mekonnen, Z. A., Grant, R. F., and Schwalm, C.: Contrasting changes in gross primary productivity of different regions of North America as affected by warming in recent decades, Agric. For. Meteorol., 218, 50–64, https://doi.org/10.1016/j.agrformet.2015.11.016, 2016.

North, G. R., Bell, T. L., Cahalan, R. F., and Moeng, F.: Sampling errors in the estimation of empirical orthogonal functions, Mon. Weather Rev., 110, 699–706, https://doi.org/10.1175/1520-0493(1982)110<0699:SEITEO>2.0.CO;2, 1982.

Park, J.-H., An, S.-I., and Kug, J.-S.: Interannual variability of western North Pacific SST anomalies and its impact on North Pacific and North America, Clim. Dyn., 49, 3787–3798, https://doi.org/10.1007/s00382-017-3538-8, 2017.

Ren, H., Jin, F., Tian, B., and Scaife, A. A.: Distinct persistence barriers in two types of ENSO, Geophys. Res. Lett., 43, 10973–10979, https://doi.org/10.1002/2016GL071015, 2016.

Saji, N. H., Goswami, B. N., Vinayachandran, P. N., and Yamagata, T.: A dipole mode in the tropical Indian Ocean, Nature, 401, 360–363, https://doi.org/10.1038/43854, 1999.

Schwartz, M. D. and Reiter, B. E.: Changes in North American spring, Int. J. Climatol., 20, 929–932, https://doi.org/10.1002/1097-0088(20000630)20:8<929::AID-JOC557>3.0.CO;2-5, 2000.

Seager, R. and Vecchi, G. A.: Greenhouse warming and the 21st century hydroclimate of southwestern North America, P. Natl. Acad. Sci. USA, 107, 21277–21282, https://doi.org/10.1073/pnas.0910856107, 2010.

Shapley, L. S.: A Value for n-Person Games, in: Contributions to the Theory of Games (AM-28), vol. 2, edited by: Kuhn, H.

W. and Tucker, A. W., Princeton University Press, 307–318, https://doi.org/10.1515/9781400881970-018, 1953.

Sheng, C., Zhang, S. Y., Liu, Y. M., Wu, G. X., and He, B.: Interannual impact of tropical southern Atlantic SST on surface air temperature over East Asia during boreal spring, npj Clim. Atmos. Sci., 6, 186, https://doi.org/10.1038/s41612-023-00515-y, 2023.

Soulard, N. and Lin, H.: The spring relationship between the Pacific-North American pattern and the North Atlantic Oscillation, Clim. Dynam., 48, 619–629, https://doi.org/10.1007/s00382-016-3098-3, 2017.

Sun, C., Kucharski, F., Li, J. P., Wang, K. C., Kang, I., Lian, T., Liu, T., Ding, R. Q., and Xie, F.: Spring Aleutian Low Weakening and Surface Cooling Trend in Northwest North America During Recent Decades, J. Geophys. Res.-Atmos., 124, 12078–12092, https://doi.org/10.1029/2019JD031405, 2019.

Sung, M.-K., Jang, H.-Y., Kim, B.-M., Yeh, S.-W., Choi, Y.-S., and Yoo, C.: Tropical influence on the North Pacific Oscillation drives winter extremes in North America, Nat. Clim. Change, 9, 413–418, 2019.

Takahashi, K., Montecinos, A., Goubanova, K., and Dewitte, B.: ENSO regimes: Reinterpreting the canonical and Modoki El Niño, Geophys. Res. Lett., 38, L10704, https://doi.org/10.1029/2011GL047364, 2011.

Tian, Q., Yu, J.-Y., Nnamchi, H. C., Li, T., Li, J. P., Li, X. C., and Ding, R. Q.: Unraveling the mystery of recent shortened response time of ENSO to Atlantic forcing, Nat. Commun., 16, 5884, https://doi.org/10.1038/s41467-025-61130-4, 2025.

Trenberth, K. E. and Hurrell, J. W.: Decadal atmosphere-ocean variations in the Pacific, Clim. Dynam., 9, 303–319, https://doi.org/10.1007/BF00204745, 1994.

Wang, B. and An, S.-I.: A method for detecting season-dependent modes of climate variability: S-EOF analysis, Geophys. Res. Lett., 32, L15710, https://doi.org/10.1029/2005GL022709, 2005.

Wang, X. H., Piao, S. L., Ciais, P., Li, J. S., Friedlingstein, P., Koven, C., and Chen, A. P.: Spring temperature change and its implication in the change of vegetation growth in North America from 1982 to 2006, P. Natl. Acad. Sci. USA, 108, 1240–1245, https://doi.org/10.1073/pnas.1014425108, 2011.

Wang, Z. B., Wu, R. G., Duan, A. M., and Qu, X.: Influence of Eastern Tibetan Plateau Spring Snow Cover on North American Air Temperature and Its Interdecadal Change, J. Clim., 33, 5123–5139, https://doi.org/10.1175/JCLI-D-19-0455.1, 2020.

Wei, T., Sun, C., and Li, J. P.: Seasonal Predictability of North American Surface Temperature Arises from SST Propagation over the Western Pacific, J. Clim., 36, 6273–6286, https://doi.org/10.1175/JCLI-D-22-0783.1, 2023.

Xie, S.-P. and Carton, J. A.: Tropical Atlantic Variability: Patterns, Mechanisms, and Impacts, in: Earth's Climate: The Ocean–Atmosphere Interaction, vol. 147, edited by: Wang, C., Xie, S. P., and Carton, J. A., American Geophysical Union, Washington, D. C., 121–142, https://doi.org/10.1029/147GM07, 2004.

Xue, Y., Diallo, I., Li, W., David Neelin, J., Chu, P. C., Vasic, R., Guo, W. D., Li, Q., Robinson, D. A., Zhu, Y. J., Fu, C. B., and Oaida, C. M.: Spring Land Surface and Subsurface Temperature Anomalies and Subsequent Downstream Late Spring-Summer Droughts/Floods in North America and East Asia, J. Geophys. Res.-Atmos., 123, 5001–5019, https://doi.org/10.1029/2017JD028246, 2018.

Zhang, W. J. and Jiang, F.: Subseasonal Variation in the Winter ENSO-NAO Relationship and the Modulation of Tropical North Atlantic SST Variability, Climate, 11, 47, https://doi.org/10.3390/cli11020047, 2023.

Zhong, W. G. and Wu, Z. W.: Subseasonal variations of Eurasian wintertime surface air temperature: two distinct leading modes, Clim. Dynam., 59, 85–108, https://doi.org/10.1007/s00382-021-06118-8, 2022.

Zhong, W. G. and Wu, Z. W.: Subseasonal strength reversal of the East Asian winter monsoon, Clim. Dynam., 61, 709–727, https://doi.org/10.1007/s00382-022-06610-9, 2023.

Zhong, W. G. and Wu, Z. W.: Forecasting East Asian winter temperature via subseasonal predictable mode analysis, Clim. Dynam., 62, 277–297, https://doi.org/10.1007/s00382-023-06916-2, 2024.